

Original citation:

Pastor-Fernandez, Carlos, Bruen, Thomas, Widanage, Widanalage Dhammika, Gama-Valdez, M. A. and Marco, James. (2016) A study of cell-to-cell interactions and degradation in parallel strings : implications for the battery management system. Journal of Power Sources, 329 . pp. 574-585.

Permanent WRAP URL:

<http://wrap.warwick.ac.uk/81616>

Copyright and reuse:

The Warwick Research Archive Portal (WRAP) makes this work of researchers of the University of Warwick available open access under the following conditions.

This article is made available under the Creative Commons Attribution 4.0 International license (CC BY 4.0) and may be reused according to the conditions of the license. For more details see: <http://creativecommons.org/licenses/by/4.0/>

A note on versions:

The version presented in WRAP is the published version, or, version of record, and may be cited as it appears here.

For more information, please contact the WRAP Team at: wrap@warwick.ac.uk



A Study of Cell-to-Cell Interactions and Degradation in Parallel Strings: Implications for the Battery Management System



C. Pastor-Fernández^{a,*}, T. Bruen^a, W.D. Widanage^a, M.A. Gama-Valdez^b, J. Marco^a

^a WMG, University of Warwick, Coventry, CV4 7AL, UK

^b Jaguar Land Rover, Banbury Road, Warwick, CV35 0XJ, UK

HIGHLIGHTS

- Experimental evaluation of SoH within parallel connected cells aged differently.
- Current, SoC and cell temperature drive SoH cell-to-cell convergence.
- An initial 45% difference in cell-to-cell SoH (resistance) converges to 30%.
- An initial 40% difference in cell-to-cell SoH (capacity) converges to 10%.
- A linear correlation between capacity fade and resistance increase is observed.

ARTICLE INFO

Article history:

Received 6 June 2016

Received in revised form

23 July 2016

Accepted 31 July 2016

Keywords:

Lithium ion technology

Battery pack

Battery management system

State of health estimation

ABSTRACT

Vehicle battery systems are usually designed with a high number of cells connected in parallel to meet the stringent requirements of power and energy. The self-balancing characteristic of parallel cells allows a battery management system (BMS) to approximate the cells as one equivalent cell with a single state of health (SoH) value, estimated either as capacity fade (SoH_E) or resistance increase (SoH_P). A single SoH value is however not applicable if the initial SoH of each cell is different, which can occur when cell properties change due to inconsistent manufacturing processes or in-homogeneous operating environments. As such this work quantifies the convergence of SoH_E and SoH_P due to initial differences in cell SoH and examines the convergence factors. Four 3 Ah 18650 cells connected in parallel at 25 °C are aged by charging and discharging for 500 cycles. For an initial SoH_E difference of 40% and SoH_P difference of 45%, SoH_E converge to 10% and SoH_P to 30% by the end of the experiment. From this, a strong linear correlation between ΔSoH_E and ΔSoH_P is also observed. The results therefore imply that a BMS should consider a calibration strategy to accurately estimate the SoH of parallel cells until convergence is reached.

© 2016 Published by Elsevier B.V.

1. Introduction

In recent years lithium-ion (Li-ion) cells in a battery pack have become the favourable choice for electric power transportation systems. In order to increase the pack capacity and meet requirements for power and energy, cells in a battery module are often electrically connected in parallel [1]. For instance, each unit of the BMW E-Mini 35 kWh battery pack is composed of 53 cells connected in parallel and 2 in series. Two units constitutes a module and the whole battery is composed of 48 modules connected in series [2]. Another example is the Tesla Model S 85 kWh

battery pack. This battery pack includes 16 modules of 6S74P configuration (6 cells connected in series and 74 cells connected in parallel) summing to 7104 cells within the complete battery assembly [3].

Battery health diagnosis is essential to develop a control strategy in order to ensure safe and lifetime efficient operation of electric and hybrid vehicles. State of Health (SoH) is the parameter used by the Battery Management System (BMS) to monitor battery ageing. SoH is often calculated based on two metrics: capacity fade and power fade [4]. These metrics are directly related to vehicle level attributes that limit driving range and vehicle power, respectively. For the case where cells are connected in parallel, the BMS typically does not monitor the SoH of each individual cell because the BMS does not have access to individual cell currents

* Corresponding author.

E-mail address: c.pastor-fernandez@warwick.ac.uk (C. Pastor-Fernández).

and temperatures. Thus, the BMS cannot determine the capacity fade and power fade at cell level. For this case the BMS approximates the SoH as that of an equivalent single value for the whole battery stack. This approximation is based on the assumption that the SoH of cells connected in parallel are the same since they have identical terminal voltages. This assumption is however no longer valid when cell properties change due to manufacturing tolerances and usage conditions. For instance, the presence of temperature gradients or the existence of different resistance paths that will underpin an uneven current distribution within the system represent typical scenarios where cell-to-cell SoH may be different. Such an imbalanced scenario has been previously examined in Refs. [5–8]. Another potential application of this study is second life grid storage modules connected in parallel as suggested in Refs. [9,10].

In a recent study, Gogoana et al. [5] cycled two cylindrical lithium-iron phosphate (LFP) cells connected in parallel to evaluate the degradation of each cell over time. They identified that an initial 20% discrepancy in internal resistance between cells in a parallel string results in a 40% reduction of the total cycle life. They attributed this result to the uneven high currents experienced by each cell.

Gong et al. [6] cycled four groups of Li-ion cells. Each group of cells was composed of two cells with different degradation levels. They showed that when two cells with a 20% impedance difference were connected in parallel, the peak current experienced was 40% higher than if the cells had the same impedance.

Zhang et al. [7] cycled two 26650 LFP cells connected in parallel, with each cell at a different temperature (5 °C and 25 °C). Based on a simplified thermal-electrochemical model, it was shown that temperature differences between the cells makes self-balancing difficult, which consequently accelerates battery degradation.

Shi et al. [8] cycled two groups of LFP batteries (each one composed of two cells) for cycle life and basic performance analysis. The first group was tested at 25 °C, whereas the second group was tested at 25 °C and 50 °C to evaluate the effect of high temperature. They concluded that imbalanced currents can directly affect the capacity fade rate of cells connected in parallel.

These studies highlight that cells connected in parallel will age differently when the SoH of each individual cell is not the same. These results raise the question as to whether the BMS will estimate the SoH correctly under this situation. The contribution of this work is to find an answer for this question quantifying the cell-to-cell SoH for a scenario when each initial cell SoH is different. To understand the reasons behind the cell-to-cell SoH variation, SoC, current and temperature distribution in the short-term, and charge-throughput and thermal energy in the long-term are examined. A simple SoH diagnosis and prognosis approach is also presented, where capacity and resistance, and the change in SoH_E (based on a measure of the cell capacity) and the change in SoH_P (based on a measure of the cell resistance) are approximated by a linear relationship. The overall output of this work is expected to improve the accuracy of SoH diagnosis and prognosis functions within the BMS when cells are connected in parallel.

The structure of this work is divided as follows: Section 2 explains the most common definitions used in the literature for SoH capacity fade (SoH_E) and power fade (SoH_P). Section 3 summarises the experiment where four commercially available 3 Ah 18650 lithium-ion cells connected in parallel were aged by 500 cycles. The results are given in Section 4, where the factors which drive the SoH convergence are evaluated. Based on the results for capacity and resistance fade, Section 5 proposes a simple approach for SoH diagnosis and prognosis based on a linear correlation between capacity and resistance, and between the change in SoH_E (ΔSoH_E) and the change in SoH_P (ΔSoH_P). Finally, the limitations of this

study and further work are stated in Section 6 and conclusions are presented in Section 7.

2. SoH definition

SoH diagnosis and prognosis is essential to ensure effective control and management of Li-ion Batteries (LIBs). The SoH will evolve differently depending on the battery state: cycling or storage [11]. The SoH depends also on different parameters which can be controlled by the BMS. For automotive applications these parameters are typically battery temperature, Depth of Discharge (DoD), discharging and charging current rates for cycling, and the SoC employed for storage conditions [4]. Since the SoH depends on different parameters it is difficult to estimate the contribution of each parameter. The SoH has an upper and a lower limit: Begin of Life (BoL) and End of Life (EoL). BoL (SoH = 100%) represents the state when the battery is new, and EoL (SoH = 0%) is defined as the condition when the battery cannot meet the performance specification for the particular application for which it was designed [13]. In essence, EoL corresponds to the battery End of Warranty (EoW) period, adopted in some automotive standards [14,15]. In relation to capacity and resistance, the EoL values are commonly defined as [4,11–13]:

$$C_{EoL} = 0.8 \cdot C_{BoL} \quad (1)$$

$$R_{EoL} = 2 \cdot R_{BoL} \quad (2)$$

According to [4] and [11–13], SoH_E and SoH_P are often calculated as a percentage with respect to the difference between BoL and EoL in either capacity (Equation (3)) or resistance (Equation (4)).

$$\begin{aligned} SoH_E &= \frac{C_{now} - C_{EoL}}{C_{BoL} - C_{EoL}} \cdot 100 = \frac{C_{now} - 0.8 \cdot C_{BoL}}{C_{BoL} - 0.8 \cdot C_{BoL}} \cdot 100 \\ &= \frac{C_{now} - 0.8 \cdot C_{BoL}}{0.2 \cdot C_{BoL}} \cdot 100 \end{aligned} \quad (3)$$

$$\begin{aligned} SoH_P &= \frac{R_{now} - R_{EoL}}{R_{BoL} - R_{EoL}} \cdot 100 = \frac{R_{now} - 2 \cdot R_{BoL}}{R_{BoL} - 2 \cdot R_{BoL}} \cdot 100 \\ &= \left(2 - \frac{R_{now}}{R_{BoL}} \right) \cdot 100 \end{aligned} \quad (4)$$

The decision as to which measure of battery health to use, SoH_E, SoH_P or both, depends on the application. In the case of the automotive industry SoH_E is commonly employed in high-energy applications such as BEVs (specific energy >150 Wh/kg) [16], SoH_P is used for high-power applications such as Hybrid Electric Vehicles (HEVs) (specific power > 1500 W/kg) [16] and both metrics can be combined for Plug-in-HEV (PHEV) applications.

3. Experimental procedure

This study extends the experiment performed in [1], where four 3 Ah 18650 Li-ion cells were aged by 0, 50, 100 and 150 cycles individually to ensure an initial SoH_E difference of 40% and SoH_P difference of 45% between the least and the most aged cells. These values correspond to a difference of capacity and impedance of circa 8% and 30% respectively. Research published highlights that differences in cell properties from initial manufacture and integration may be circa 25% for impedance [5] and 9% for capacity [17], which is in agreement with the initial differences considered in this study. The four cells are then connected in parallel and cycled for a total of 500 cycles, where 500 cycles represents the EoL state according to the manufacturer's specifications. Thus, all the cells were loaded at least for 500 cycles. The experimental procedure is

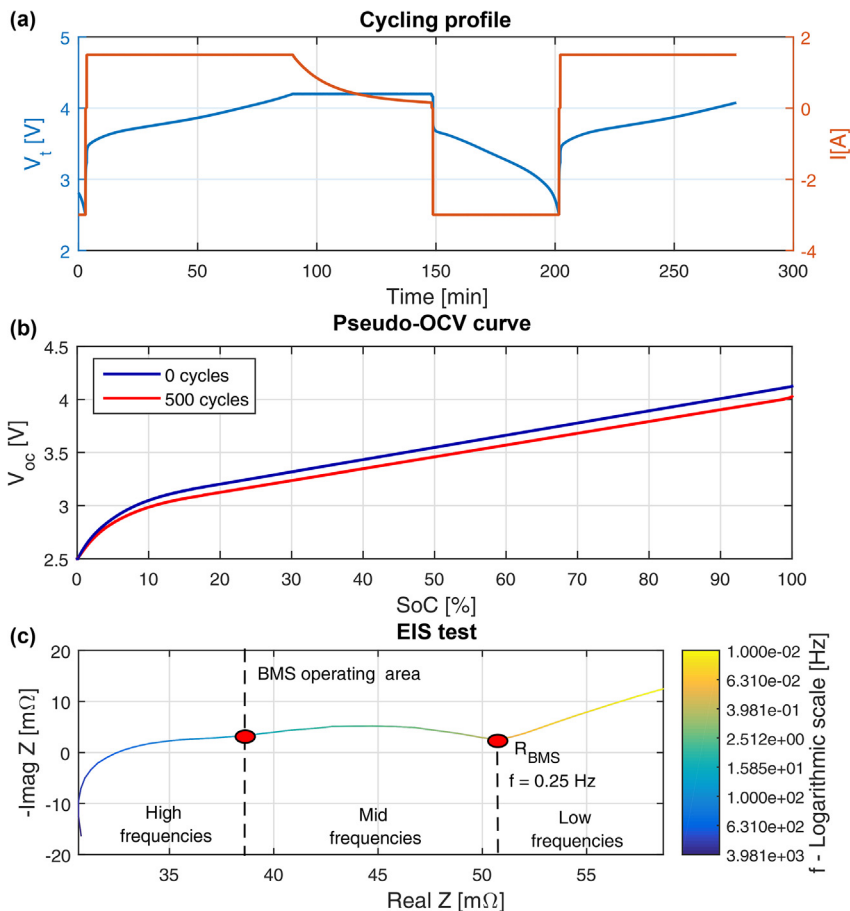


Fig. 1. (a) Charge-discharge cycling profile employed to age the cells, (b) Pseudo-OCV-SoC curve of cell 1 for 0 and 500 cycles for a discharge event, (c) EIS test with respect to the frequency showing BMS operating area and R_{BMS} .

divided into two phases: cycle ageing and cell characterisation. Table 1 shows the test that was performed. The following subsections summarise each of these tests. For a more detailed explanation, refer to [1].

3.1. Cycle ageing

As illustrated in Fig. 1(a) cycle ageing involved repeated cycles at constant ambient temperature of $25\text{ }^{\circ}\text{C} \pm 1\text{ }^{\circ}\text{C}$ of the following: a 1C discharge until the lower voltage limit was reached followed by Constant Current-Constant Voltage (CC-CV) charging protocol. The CC phase involved charging the cell at $C/2$ until the end of charge voltage (4.2 V) was reached. The CV phase then consisted of charging the cell until the current fell to $C/20$ (150 mA). This profile was selected to significantly age the cells whilst not exceeding the

manufacturer's operating cell specification. This was achieved by cycling the cells with a full DoD (e.g. 0–100%) without using large currents [1]. A large DoD is deemed to emulate the operation of a typical BEV in which, as discussed within [1], the BMS will control a large variation in SoC to further maximise the range of the vehicle.

During cycle ageing, each cell was connected in series with a 10 m Ω shunt resistor over which the voltage was measured. The current was then calculated based on a current-voltage relationship obtained through a least-squares solution in Ref. [1]. In addition, the temperature was also measured midway along its length of each cell using type T thermocouples.

3.2. Cell characterisation

Cell characterisation includes three tests: capacity test, pseudo-

Table 1
Experimental test matrix.

Cell	Test	Test start ^a [#cycles]	Test finish [#cycles]	Testing procedure	T [$^{\circ}\text{C}$]	ΔDoD [%]	t_{samp} [s]
1	Cycling	0	500	CC-CV chg and 1C dchg	25	100	1
	Charact	Every 50 cycles		1C dchg, EIS test and pseudo-OCV	25	100	1
2	Cycling	50	500	CC-CV chg and 1C dchg	25	100	1
	Charact	Every 50 cycles		1C dchg, EIS test and pseudo-OCV	25	100	1
3	Cycling	100	500	CC-CV chg and 1C dchg	25	100	1
	Charact	Every 50 cycles		1C dchg, EIS test and pseudo-OCV	25	100	1
4	Cycling	150	500	CC-CV chg and 1C dchg	25	100	1
	Charact	Every 50 cycles		1C dchg, EIS test and pseudo-OCV	25	100	1

^a Initial testing was performed in Ref. [1].

OCV test and EIS test. In order to track the aged state of each cell over time, each of these tests was performed every 50 cycles. In total, each cell was characterised 11 times.

- The capacity test determines the quantity of electric charge that a battery can deliver under specified discharge conditions. Firstly each cell was charged to 100% SoC according to CC-CV protocol. Then, the cell was discharged at 1 C to the lower voltage limit. The cell's capacity is defined as the charge dissipated over this discharge event.
- The pseudo-OCV test is performed by discharging from the upper cell voltage threshold (4.2 V) to the lower cell voltage threshold (2.5 V) at C/10. The corresponding pseudo-OCV curve is related to the SoC and is shown for cell 1 for 0 and 500 cycles in Fig. 1(b).
- The EIS test was performed in galvanostatic mode with a peak current amplitude of 150 mA (C/20) using a Solartron modulated system (model 2100A). The tests were performed between 2 mHz and 100 kHz at SoC = 20%, SoC = 50% and SoC = 90%. SoC was adjusted based on the pseudo-OCV curve (refer to Fig. 1(b)). According to [18], a period of 4 h was allowed prior to performing each EIS test. This measure avoids changes in the internal impedance when the cells are halted after being excited. Operation at high frequencies (≥ 2.5 kHz) would increase substantially the cost of the BMS hardware because the required sampling rate will be higher. This explains why a BMS will typically only operates at mid and low frequencies (< 100 Hz). As such, the resistance considered for this work is the one that the BMS is capable of measuring. This resistance is here named as a

BMS resistance (R_{BMS}) and, it is represented by the mid-frequency turning point of the EIS plot as illustrated in Fig. 1(c). This approach is consistent with other studies reported within the literature [1], [19].

4. Results and discussions

4.1. Capacity – SoH_E and resistance – SoH_P

Fig. 2(a) and (b) illustrate the degradation of each cell over time based on the measurement of the capacity at 1 C and the R_{BMS} at an SoC of 50%.

Fig. 2(a) and (b) indicate that capacity and R_{BMS} tends to converge for cells 2, 3 and 4 over cycle number. Since cell 1 represents the least aged cell, it requires more time to converge at the same level than the rest of the cells. Fig. 2(c) and (d) show that the resulting SoH_E and SoH_P trend is similar to the capacity and R_{BMS} trend. It can be seen that the SoH_P decreases faster than SoH_E reaching the EoL value earlier (between 200 and 350 cycles) than the value specified by the manufacturer (500 cycles). This result indicates the lifetime power capability of the cells is shorter than the energy capability. SoH_P decreases faster than SoH_E because the conditions at which the cells were cycled (1C-rate discharge and $\Delta DoD = 100\%$) leads to significant power losses. Such a cell would not meet a commercial viable battery specification where both metrics, SoH_E and SoH_P , need to be positive until the EoW period is reached.

Fig. 2(c) and (d) also illustrate the mean value of the SoH. This value represents the equivalent SoH that the BMS would track. A

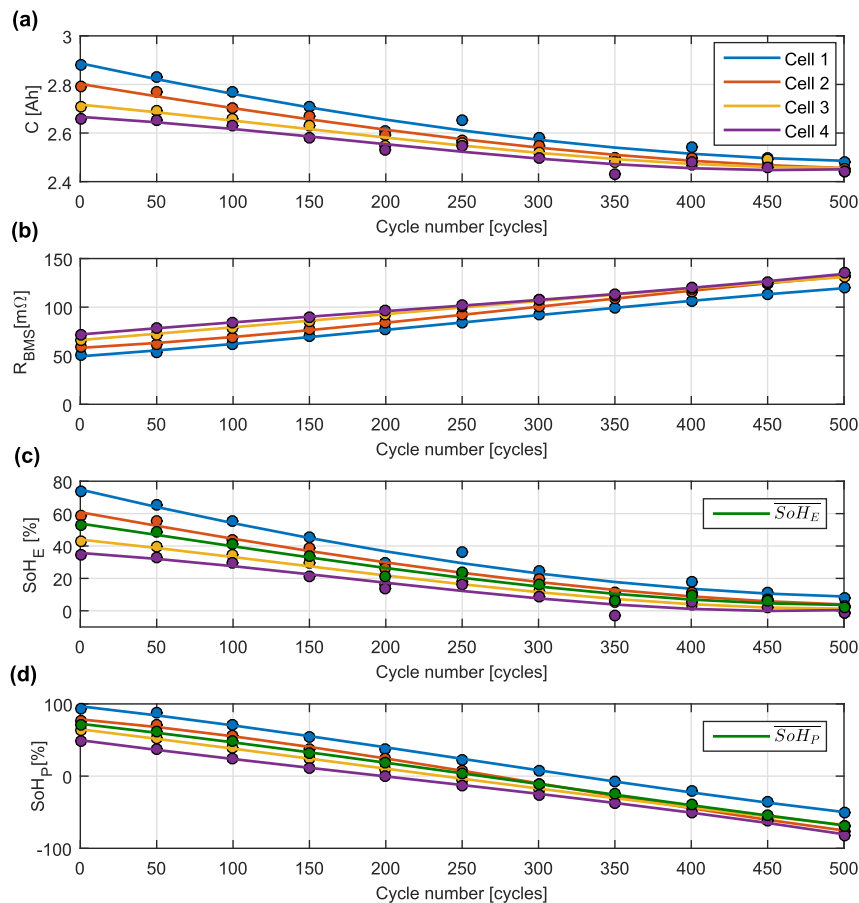


Fig. 2. (a) Cell capacity over cycle number, (b) Cell R_{BMS} (SoC 50%) over cycle number, (c) Cell SoH_E and $\overline{SoH_E}$ over cycle number, and (d) Cell SoH_P and $\overline{SoH_P}$ over cycle number.

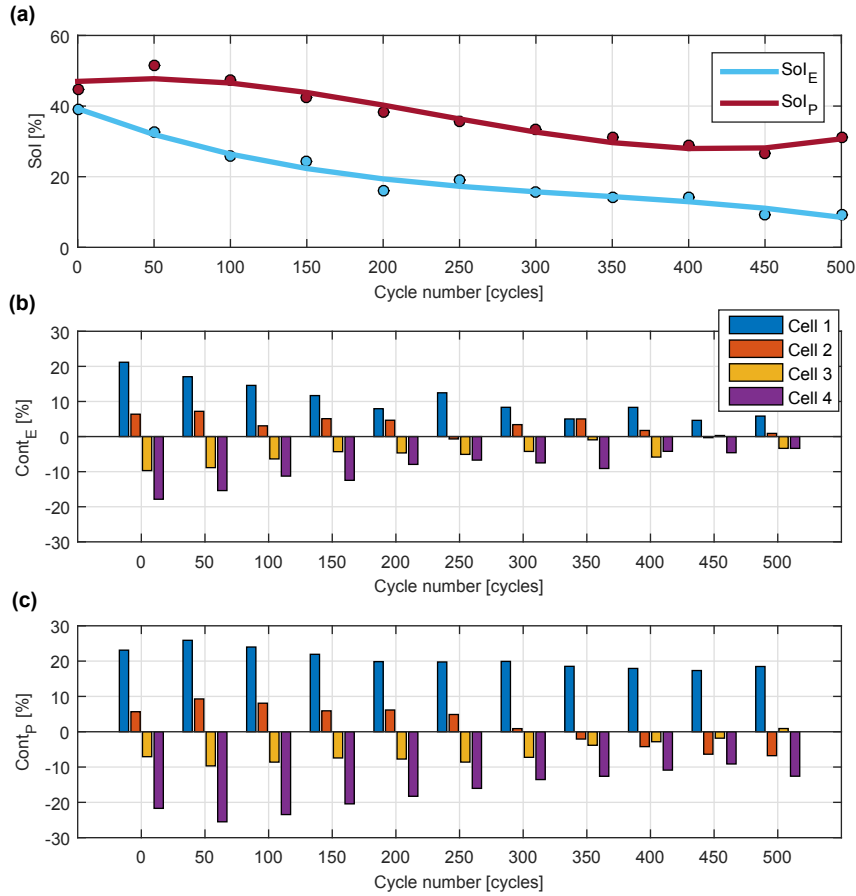


Fig. 3. (a) Sol_E and Sol_P over cycle number, (b) Cell $Cont_E$ over cycle number and (c) Cell $Cont_P$ over cycle number.

new metric called State of Imbalance (Sol) is defined to quantify the maximum cell-to-cell SoH difference at each characterisation test k . The Sol is calculated for the case of SoH_E and SoH_P as shown Equation (5) and Equation (6).

$$Sol_E^k = \max(SoH_E^k) - \min(SoH_E^k) \quad (5)$$

$$Sol_P^k = \max(SoH_P^k) - \min(SoH_P^k) \quad (6)$$

$$k = 1 \dots 11$$

Fig. 3(a) illustrates that Sol_P decreases less than the Sol_E . For an initial Sol_E of 40% and Sol_P of 45%, Sol_E decreases to 10% and Sol_P to 30% by the end of the test. In order to study which cell contributes more to the SoH convergence Fig. 3(b) and (c) show the difference of each cell SoH_E and SoH_P with respect to the mean value illustrated in Fig. 2(c) and (d), respectively. $Cont_E$ and $Cont_P$ of each cell i at each characterisation test k is computed using Equation (7) and Equation (8).

$$Cont_{E_i}^k = SoH_{E_i}^k - \overline{SoH_{E_i}^k} \quad (7)$$

$$Cont_{P_i}^k = SoH_{P_i}^k - \overline{SoH_{P_i}^k} \quad (8)$$

$$k = 1 \dots 11, \quad i = 1 \dots 4$$

Fig. 3(b) and (c) show cell 1, the least aged cell, contributes more

to the convergence whilst cell 4, the most aged cell, contributes the least. The $Cont_E$ and $Cont_P$ decreases with cycle number, outlining the SoH of each cell tends to converge.

4.2. Driving factors for SoH convergence

4.2.1. Current and charge-throughput distribution

Previous work [1] showed that cells connected in parallel under imbalanced scenarios can undergo significantly different currents, contributing to the cells degrading differently. To understand the variation of the individual cell currents when the cells are connected in parallel a simplified cell model was here considered. This model comprises an OCV voltage source V_{oc} connected in series with an internal cell resistance R_{int} . Previous literature [1,12,18,19] use this model with an added RC parallel branch to capture diffusion effects. The RC parallel combination is herein neglected to help explain the cell-to-cell SoH variation more easily.

Based on this model, the individual cell current is derived as in Equation (9).

$$V_t = V_{oc} + V_R = V_{oc} + R_{int} \cdot I_{cell} \rightarrow I_{cell} = \frac{V_t - V_{oc}}{R_{int}} \quad (9)$$

The wide SoC range and difference in cell SoH give a scenario with significant differences in V_{oc} and R_{int} which, according to Equation (9), will cause differences in cell currents.

Fig. 4(a) and (b), and Fig. 5(a) and (b) relate the individual SoC and the individual cell currents of each cell I_1 , I_2 , I_3 and I_4 for the 35th and the 435th discharge-charge cycle, respectively. These cycles were arbitrarily selected near to the beginning and the end of

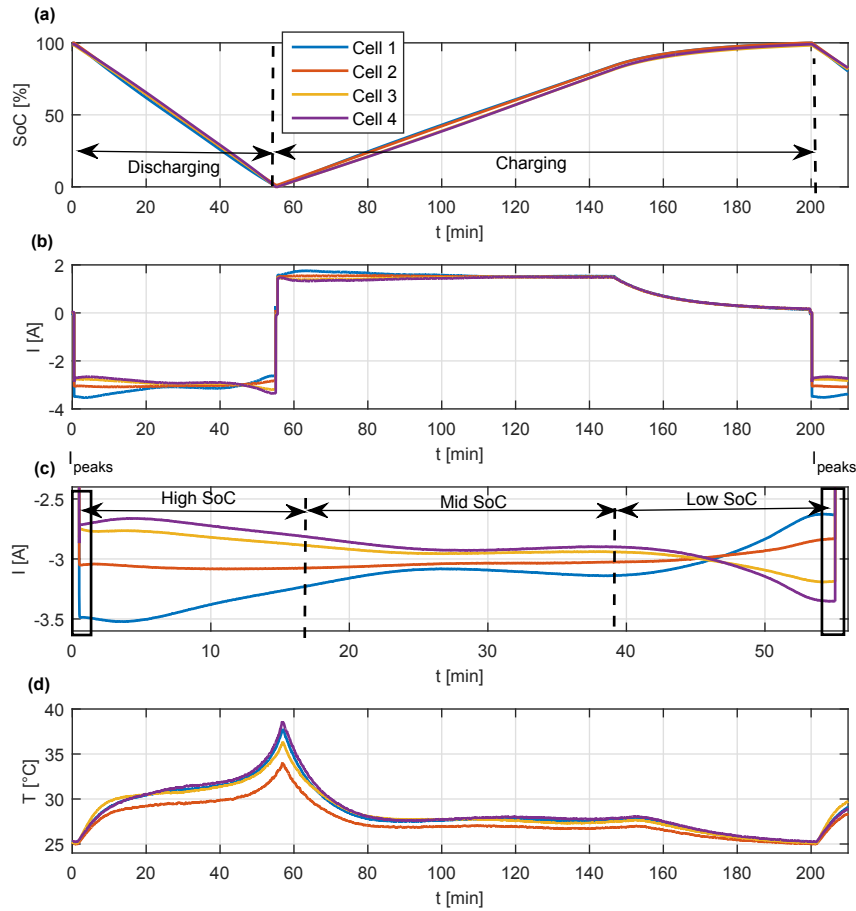


Fig. 4. (a) Individual SoC of each cell for the 35th cycle, (b) current distribution of each cell for the 35th cycle, (c) detailed view of this current distribution for the discharge event for the 35th cycle, (d) temperature distribution of each cell for the 35th cycle.

the test.

The individual current of each cell diverges more for the discharging event than for the charging event because the magnitude of the C-rate is larger for discharging (-1 C) than for charging ($+0.5$ C). The SoC of the less aged cells (cells 1 and 2) decreases during discharging or increases during charging faster than for the more aged cells because the current flow in the less aged cells is higher in magnitude than in the more aged cells (cells 3 and 4). Thus, when the less aged cell has completely discharged (or charged), the more aged cells have not completely discharged (or charged) completely yet, which consequently may drive higher currents in these cells.

According to [1], this uneven current distribution during charging and discharging causes peaks in the current which could lead to premature ageing of the cells. Fig. 4(c) and Fig. 5(c) illustrate the current distribution of each cell during discharge for the 35th and the 435th discharge-charge cycle, respectively. The peaks in the current are reached at low and high SoC, as a result of the deepest discharge effects of the pseudo-OCV curve (refer to Fig. 1(b)). The less aged cells take more current at high SoC as their impedance is lower than the impedance of the more aged cells. However, the more aged cells take more current at low SoC as they have been discharged slower than the less aged cells and thus their impedance is lower than the impedance of the less aged cells. According to Fig. 1(b), the V_{oc} also decreases more at low SoC that additionally limits the current that is able to flow (refer to Equation (9)). This trade-off between SoC, impedance and V_{oc} explain the cell-to-cell current cross-over depicted in Fig. 4(c) and Fig. 5(c). This result

has been previously reported in Refs. [1], [5].

Another observation from Fig. 4(c) and Fig. 5(c) is the peak-to-peak current difference between the 35th and the 435th cycle. The peak-to-peak current difference between the least and the most aged cell is larger at high SoC or low SoC for the 35th cycle (0.75 A) than for the 435th cycle (0.5 A). This convergence in the peak-to-peak current is explained by the convergence of the individual cell capacity and resistance as illustrated in Fig. 2(a) and (b).

The charge-throughput is evaluated to analyse the effect of the current distribution in the long-term. The charge-throughput is the amount of accumulated current (absolute value) that is stored (charging) and released (discharging) in the battery over time. Using Equation (10) the charge-throughput is computed as the integral of the current over the difference between the final t_f^k and the initial t_0^k time. In this case, as the cycling test is “paused” to characterise the cells, the charge-throughput (AhT) over the total cycling tests is derived as the monotonic accumulation of the charge-throughput of each individual cycling test k , one after another.

$$AhT_i^k = \sum_{k=1}^k \int_{t_0^k}^{t_f^k} |I(t)_i^k| dt \quad (10)$$

$$k = 1 \dots 11, \quad i = 1 \dots 4$$

Fig. 6(a) illustrates the charge-throughput of each cell i over

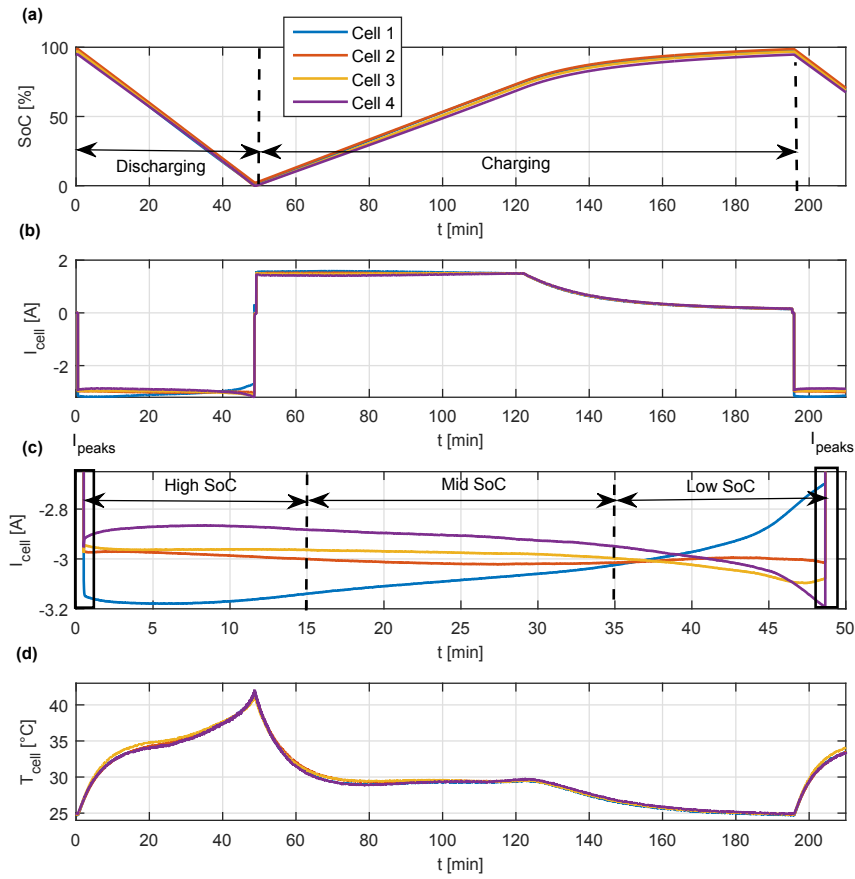


Fig. 5. (a) Individual SoC of each cell for the 435th cycle, (b) current distribution of each cell for the 435th cycle, (c) detailed view of this current distribution for the discharge event for the 435th cycle, (d) temperature distribution of each cell for the 435th cycle.

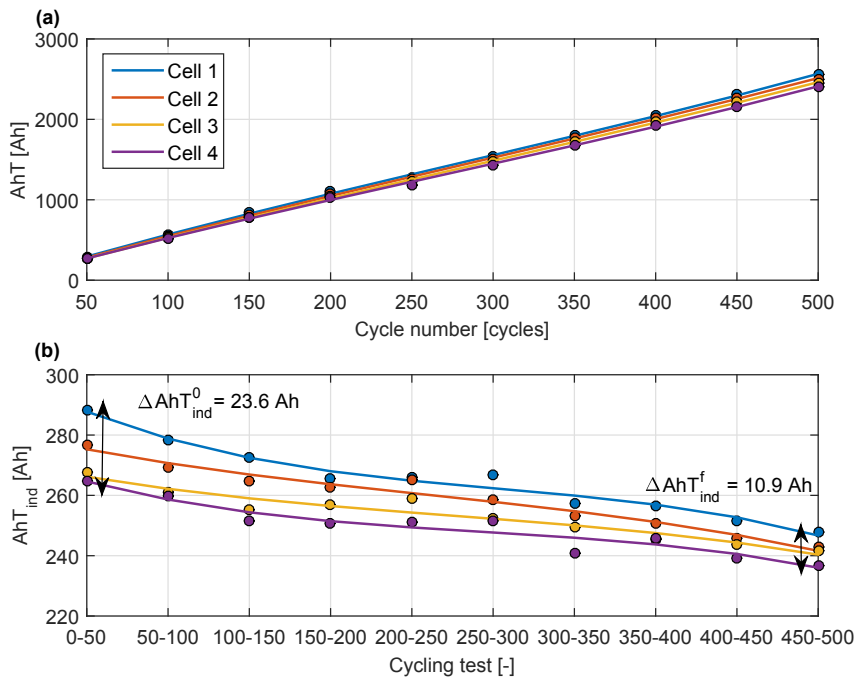


Fig. 6. (a) Accumulative charge-throughput taken by each cell over cycle number, (b) Charge-throughput taken by each cell over each cycling test.

cycle number and show that the charge-throughput of the less aged cells is larger than for the more aged cells over time, outlining the current in the less aged cells is in overall larger than in the more aged cells.

To see clearly that the charge-throughput also converges the individual charge-throughput after each cycling test is computed using Equation (11). Equation (11) is the same than Equation (10) without accumulating the charge-throughput over cycle number.

$$AhT_{i\ ind}^k = \int_{t_0^k}^{t_f^k} |I(t)_i^k| dt \quad (11)$$

$$k = 1 \dots 11, \quad i = 1 \dots 4$$

Fig. 6(b) illustrates that the individual charge-throughput after each cycling test converges. This result together with the convergence of the current (short-term) support the convergence of the SoH.

4.2.2. Temperature and thermal-energy distribution

Since cell temperature primarily depends on cell impedance and current, a number of studies correlate these parameters with SoH [1,7,8]. Fig. 4(d) and Fig. 5(d) show the temperature distribution in each cell for the 35th and the 435th charge-discharge cycle, respectively.

Fig. 4(d) and Fig. 5(d) illustrate that the cell temperature is larger for all the cells at the 435th (43 °C) than the 35th cycle (38 °C). The increase in temperature over cycle number is due to the increase of R_{BMS} as depicted in Fig. 2. This increase of temperature is more significant for low and high SoC with respect to mid SoC due to the divergence of the individual cell currents (refer to Section 4.2.1) and larger magnitude of R_{BMS} [19].

In comparison with the current depicted in Fig. 4(d) and Fig. 5(d), the variation of the temperature does not follow the initial order of ageing of each cell. Fig. 4(d) depicts that the temperature of cell 1, cell 3 and cell 4 is larger than the temperature of cell 2. This result is explained based on the relative values of the impedance of each cell with respect to the current. The difference in current of cell 1, cell 3 and cell 4 vary significantly ($\Delta I_1=0.9$ A, $\Delta I_3 = 0.42$ A and $\Delta I_4 = 0.65$ A) from the beginning to the end of the discharge, whereas the difference in current of cell 2 changes less ($\Delta I_2=0.2$ A). In addition, the change of the impedance with respect to the SoC influences also in the variation of cell temperature. For instance, since cell 1 is the least aged cell it has the lowest resistance value (refer to Fig. 2(b)). However, the impedance of cell 1 will rise at low SoCs due to the significant drop of V_{oc} (refer to Fig. 1(b)) causing an increase in temperature. The temperature of cell 2 is consistently the lowest temperature because it has a relatively low impedance without undergoing large current differences. This result is supported in Ref. [1] where cell temperature did not vary with respect to the order of ageing.

For the case of the 435th cycle, the temperature is approximately the same for all the cells since the current from the beginning to the end of the discharge change very little ($\Delta I_1=0.4$ A, $\Delta I_2 = 0.04$ A, $\Delta I_3 = 0.15$ A and $\Delta I_4 = 0.3$ A) and the resistance of each cell tend to converge (refer to cell resistance values in Fig. 2(b)). Comparing both Fig. 4(d) and Fig. 5(d) it is possible to conclude that temperature tend to converge over time.

It can also be seen that the average peak temperature at 435th cycle (41.5 °C) is larger than the average peak temperature at 35th cycle (36 °C) due to the increase of R_{BMS} with cycle number (refer to Fig. 2(b)). To evaluate the temperature convergence in the long-term Equation (12) approximates the total thermal energy

released in each cell i along the total number of cycling tests.

$$E_{th\ i}^k = \sum_{k=1}^k \int_{t_0^k}^{t_f^k} (I(t)_i^k)^2 \cdot \overline{R_{BMS\ i}^k} dt \quad (12)$$

$$k = 1 \dots 11, \quad i = 1 \dots 4$$

Where $I(t)_i^k$ denotes the current flow, and t_0^k and t_f^k the initial and the final time. Equation (13) gives $\overline{R_{BMS}^k}$ as the mean value of the instantaneous R_{BMS} for each characterisation test k and cell i considering each measured SoC.

$$\overline{R_{BMS\ i}^k} = \frac{R_{BMS\ i\ 20\%}^k + R_{BMS\ i\ 50\%}^k + R_{BMS\ i\ 90\%}^k}{3} \quad (13)$$

$$k = 1 \dots 11, \quad i = 1 \dots 4$$

The RMS value of the current is employed to simplify Equation (12) and it was calculated using Equation (14) over the charge-discharge cycle period T .

$$I_{RMS\ i}^k = \sqrt{\frac{1}{T^k} \int_{t_f^k - T^k}^{t_f^k} (I(t)_i^k)^2 dt} \quad (14)$$

$$k = 1 \dots 11, \quad i = 1 \dots 4$$

The thermal energy based on the RMS value of the current is computed using Equation (15).

$$E_{th\ i}^k = \sum_{k=1}^k (I_{RMS\ i}^k)^2 \cdot \overline{R_{BMS\ i}^k} \cdot (t_f^k - t_0^k) \quad (15)$$

$$k = 1 \dots 11, \quad i = 1 \dots 4$$

Similarly as with the charge-throughput, the thermal energy was computed as the monotonic accumulation of the thermal energy of each individual cycling test k , one after another. Fig. 7(a) demonstrates the thermal energy released by the more aged cells is larger than the thermal energy released by the less aged cells. The least aged cell (cell 1) typically undergoes the highest current, having the lowest impedance. Likewise, the most aged cell (cell 4) typically undergoes the lowest current, having the highest impedance. Thus, this result indicates the R_{BMS} contributes more to the thermal energy than the I_{RMS}^2 . To compare the contribution between R_{BMS} and I_{RMS}^2 the ratio between the R_{BMS} for cell 4 and cell 1 for each characterisation test k , and the ratio between the I_{RMS}^2 for cell 1 and cell 4 for each characterisation test k are derived using Equation (16) and Equation (17).

$$R_{r\ BMS}^k = \frac{R_{BMS\ i=4}^k}{R_{BMS\ i=1}^k} \quad (16)$$

$$I_{r\ RMS}^k = \frac{(I_{RMS\ i=1}^k)^2}{(I_{RMS\ i=4}^k)^2} \quad (17)$$

$$k = 1 \dots 11$$

Fig. 7(b) illustrates $R_{r\ BMS}^k$ is for the major part of the test larger than $I_{r\ RMS}^k$ suggesting that thermal energy is more sensitivity to

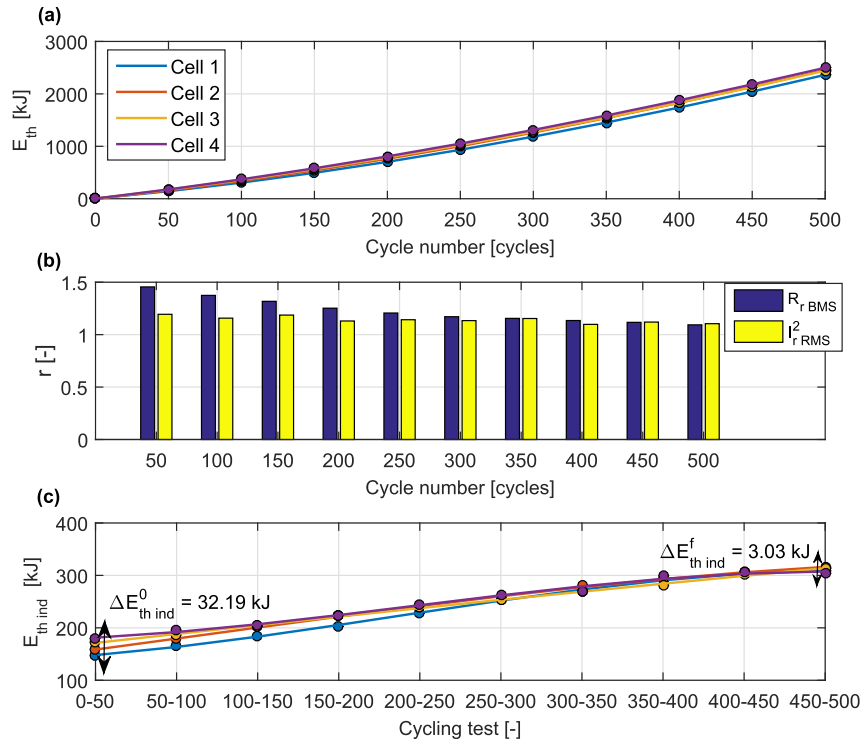


Fig. 7. (a) Total thermal energy taken by each cell over cycle number, (b) comparison between $R_{r,BMS}^k$ and $I_{r,RMS}^k$ over cycle number, (c) total thermal energy taken by each cell over each cycling test.

Table 2

Test results for the cells before and after being connected in parallel.

Cell	Test start						Test finish					
	$C^{a,b}$ [Ah]	$R_{BMS}^{a,c}$ [mΩ]	AhT^d [kAh]	E_{th}^e [kJ]	SoH_E^f [%]	SoH_p^g [%]	$C^{a,b}$ [Ah]	$R_{BMS}^{a,c}$ [mΩ]	AhT^d [kAh]	E_{th}^e [kJ]	SoH_E^f [%]	SoH_p^g [%]
1	2.88	50.72	0.00	0.00	73.68	96.54	2.54	120.00	2.55	2357.80	7.89	-50.87
2	2.79	59.04	0.00	0.00	58.88	86.58	2.50	132.04	2.50	2454.30	2.96	-76.13
3	2.71	66.66	0.00	0.00	42.81	79.30	2.47	131.37	2.45	2443.30	-1.30	-68.44
4	2.66	72.15	0.00	0.00	34.64	70.94	2.48	134.85	2.40	2493.00	-1.30	-81.94

^a Not exactly the same values as in Ref. [1] because the cells were aged due to calendar ageing between the two different tests.

^b Based on 1 C capacity test.

^c R_{BMS} measured at 50% SoC.

^d Refer to Equation (10).

^e Refer to Equation (12).

^f Refer to Equation (3).

^g Refer to Equation (4).

R_{BMS} than to I_{RMS}^2 .

To see clearly that the thermal energy also converges over time, the individual thermal energy released after each cycling test is computed using Equation (18). Equation (18) is the same than Equation (15) without accumulating the thermal energy over cycle number.

$$E_{th,ind}^k = \left(I_{RMS,i}^k \right)^2 \cdot \overline{R_{BMS,i}^k} \cdot \left(t_f^k - t_0^k \right) \quad (18)$$

$$k = 1 \dots 11, \quad i = 1 \dots 4$$

Fig. 7(c) depicts the thermal energy released by each cell over each cycling test converges. Hence, the convergence of temperature (short-term) together with the convergence of the thermal energy (long-term) support the convergence of the SoH.

As an overview, Table 2 gives a summary of the results evaluated in this section, highlighting the values at the beginning and at the

end of the experiment. Observed that the capacity and R_{BMS} of the cells before being connected in parallel differ with respect to the values reported in Ref. [1]. Since the cells were stored over half a year between the previous and this study, this difference is attributed to calendar ageing effects.

5. Simplified approach to SoH diagnosis and prognosis for cells connected in parallel

Previous studies [20,21], found that knowing the capacity allows the resistance to be approximated, and vice versa. In support of those studies Fig. 8(a), (b), (c) and (d) show a correlation between capacity and R_{BMS} for each cell. This correlation follows a linear trend since it can be approximated by a first-order polynomial fit. To measure the goodness of fit of this linear relationship the R-square value is used. The R-square can vary between 0 and 1, where 0 indicates that the model describes none of the variability of the

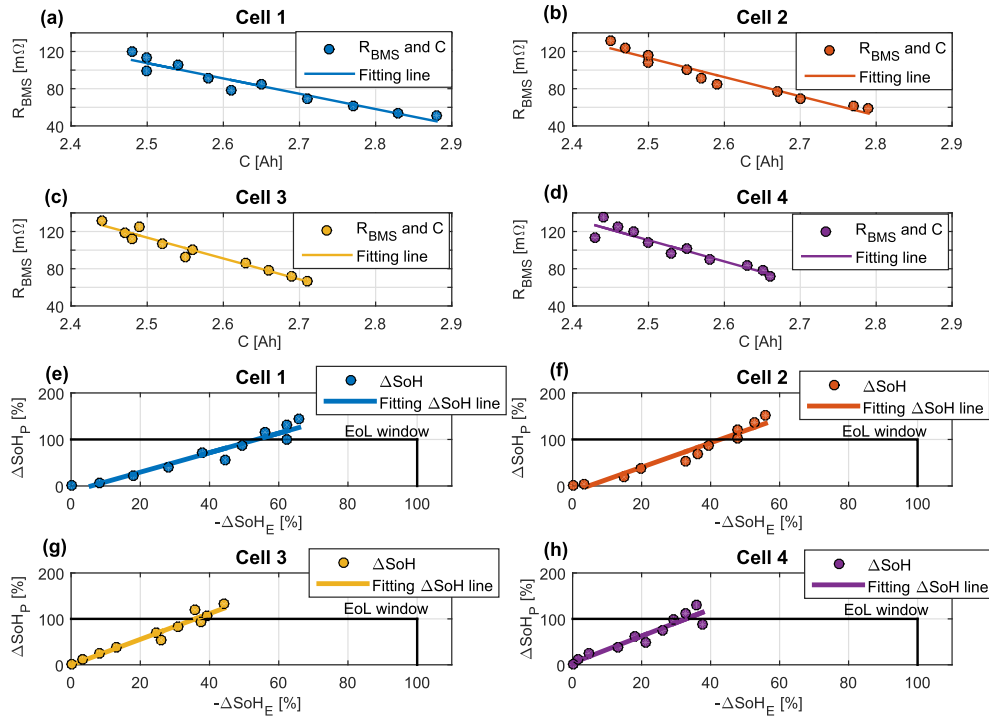


Fig. 8. Linear correlation between capacity and R_{BMS} at 50% SoC for (a) cell 1, (b) cell 2, (c) cell 3 and (d) cell 4. Linear correlation between increase in ΔSoH_E and ΔSoH_P at 50% SoC for (e) cell 1, (f) cell 2, (g) cell 3 and (h) cell 4.

response data with respect to its mean, and 1 indicates that the model relates all the variability of the response data with respect to its mean [21]. The minimum adjusted R-square value for all the cases analysed is 0.8831 for cell 4. This result implies the linear fits relate a significant variability of the response data with respect to their mean.

To estimate the change of SoH based on the capacity fade or the increase of resistance, $\Delta SoH_{E_i}^k$ and $\Delta SoH_{P_i}^k$ are calculated using Equation (19) and Equation (20). $\Delta SoH_{E_i}^k$ represents the difference between the SoH_E of each characterisation test k and each cell i ($SoH_{E_i}^k$) with respect to the SoH_E of the first characterisation test $k=1$ and each cell i ($SoH_{E_i}^1$). Similarly, $\Delta SoH_{P_i}^k$ represents the difference between the SoH_P of each characterisation test k and each cell i ($SoH_{P_i}^k$) with respect to the SoH_P of the first characterisation test $k=1$ and each cell i ($SoH_{P_i}^1$).

$$\Delta SoH_{E_i}^k = SoH_{E_i}^k - SoH_{E_i}^1 \quad (19)$$

$$\Delta SoH_{P_i}^k = SoH_{P_i}^k - SoH_{P_i}^1 \quad (20)$$

$$k = 1 \dots 11, \quad i = 1 \dots 4$$

Fig. 8(e), (f), (g) and (h) show the results for $\Delta SoH_{E_i}^k$ and $\Delta SoH_{P_i}^k$ for each cell. The relationship between $\Delta SoH_{E_i}^k$ and $\Delta SoH_{P_i}^k$ is linear for each cell and thus it is also approximated by a first-order polynomial fit. Similarly as the previous case, the minimum adjusted R-square value for all the cases analysed is 0.8831 for cell 4. It can also be seen that ΔSoH_P goes outside of the EoL threshold as it was illustrated in Fig. 2(b). Despite this, the linear relationship between ΔSoH_E and ΔSoH_P will be still valid. The only difference with respect to the result presented will be the gradient of the approximated line.

The Pearson product-moment correlation coefficient (PPMCC) is employed to quantify the grade of correlation between C and R_{BMS} ,

and ΔSoH_P and ΔSoH_E [21]. Equation (21) and Equation (22) defines the PPMCC coefficients are computed as the covariance divided by the standard deviations of each parameter using Equation (21) and Equation (22).

$$r_{R_{BMS},C} = \frac{COV_{R_{BMS},C}}{\sigma_{R_{BMS}} \cdot \sigma_C} \quad (21)$$

$$r_{\Delta SoH_P, \Delta SoH_E} = \frac{COV_{\Delta SoH_P, \Delta SoH_E}}{\sigma_{\Delta SoH_P} \cdot \sigma_{\Delta SoH_E}} \quad (22)$$

The PPMCC varies between -1 and $+1$, depending if the correlation is weak or strong. The absolute value of PPMCC is considered in order to interpret the strength of the correlation as follows. Employing the command *corrcoef* in MATLAB [22], the minimum $r_{R_{BMS},C}$ and $r_{\Delta SoH_P, \Delta SoH_E}$ is for both cases 0.9459 for cell 4. This result highlights that C and R_{BMS} , and ΔSoH_P and ΔSoH_E are strongly correlated.

The linear correlation provides sufficient justification to calculate capacity or resistance based on the knowledge of the other. Secondly, this linear correlation allows the BMS to estimate in the short-term (diagnosis) and in the long-term (prognosis) the change of SoH in a simple way, which may be further investigated in the future for real-time battery applications.

6. Limitations of this study and further work

In order to reduce the duration of the experiment, only one capacity and resistance measurement of each cell at each ageing state was considered. According to the theory of Design of Experiments (DoE) [23], more than one sample is recommended to ensure the measurements are representative. Thus, a greater sample size is necessary to increase confidence in the findings of this study.

The results of this study are only valid for the described

experimental conditions. In cases where the testing conditions change (e.g. ambient temperature or C-rate); or, the number of cells connected in parallel is different than four; or, the conditions at which the cells were initially aged are different; then, the convergence may not be reached or may be reached earlier or later. For instance, if the C-rate is high (≥ 1.5 C), then the least aged cell could undergo more current than the maximum current specified by the cell's manufacturer. This could ultimately result in a cell failure. Another example is that the number of cells connected in parallel may be related to the time required for the cells to converge. Therefore, the same study at different experimental conditions would need to be investigated in the future.

Similarly, the correlation between the capacity and R_{BMS} , and the change in SoH_E (ΔSoH_E) and SoH_P (ΔSoH_P) could also be non-linear for other test conditions, for instance, when cycling and storage conditions are combined. Hence, the applicability of this should also be tested against other testing conditions (cycling and storage) and other cell chemistries.

7. Conclusions

This work analysed the cell-to-cell SoH variation of four 3 Ah 18650 Li-ion cells connected in parallel. The SoH is defined by the capacity fade SoH_E , and the power fade SoH_P . For an initial SoH_E difference of 40% at the beginning of the test, the cells SoH_E converge to 10% at the end of the test (500 cycles). For the case of the SoH_P for an initial difference of 45% the cells converge to within 30% at the end of the test. The initial SoH_P and SoH_E corresponds to a difference of circa 30% in impedance and 8% in capacity, values which are in agreement with potential differences in cell properties from initial manufacture and integration [5,17]. This study highlights that the BMS would track an incorrect value of the SoH until the convergence is reached. To understand the reasons behind the SoH convergence, the distribution of the SoC, current, temperature, charge-throughput and thermal energy were studied. The distribution of the cell currents does not entirely depend on the initial ageing state of each cell as it is commonly assumed. The variation depends on the OCV-SoC relationship and the change of cell impedance with respect to SoC. This non-linearity in the variation of the current may cause uneven heat generation within a pack, which may require a higher specification thermal management system [1]. In comparison with the current distribution, the variation of the SoC and the temperature is less dynamic. Although these parameters change differently, all of them tend to converge over time, driving the convergence of SoH. The charge-throughput and the thermal energy of each cell over 500 cycles was also studied to analyse variation of the current and the temperature in the long-term. Similarly as for the current and the temperature, the charge-throughput and the thermal energy tend to converge over time.

This work also shows that the magnitude of the SoH decreases much faster for the case of the SoH_P with respect to the SoH_E because the testing conditions employed to cycle the cells (1 C discharge and $\Delta DoD = 100\%$) leads to significant power fade.

In addition, this work suggested a simple approach for SoH diagnosis and prognosis within the BMS. This approach was based on two linear correlations: one between the capacity and R_{BMS} , and the other between the change in SoH_E (ΔSoH_E) and SoH_P (ΔSoH_P) with a minimum adjusted R-square value of 0.8831 for both cases. This result is relevant for two main reasons. Firstly, it is only necessary to measure one parameter to estimate the other. Secondly, it could be further used to estimate the EoL of the battery. This would also require the analysis of the correlation under other conditions (e.g. temperature, C-rate, SoC and ΔDoD) in order to

cover the whole cycling spectra that a commercial battery pack may be subject to.

Acknowledgements

The research presented within this paper is supported by the Engineering and Physical Science Research Council (EPSRC - EP/I01585X/1) through the Engineering Doctoral Centre in High Value, Low Environmental Impact Manufacturing. The research was undertaken in the WMG Centre High Value Manufacturing Catapult (funded by Innovate UK) in collaboration with Jaguar Land Rover. Details of additional underlying data in support of this article and how interested researchers may be able to access it can be found here: <http://wrap.warwick.ac.uk/81110>.

The authors would like to thank Dr. Gael H. Chouchelamane, Dr. Mark Tucker and Dr. Kotub Uddin for the support on the experimental measurements and analysis of the results.

Nomenclature

Abbreviation

BEV	Battery Electric Vehicle
BMS	Battery Management System
BoL	Begin of Life
CC-CV	Constant Current Constant Voltage
chg	Charge
Charac	Characterisation
dchg	Discharge
DoD	Depth of Discharge
DoE	Design of Experiment
EIS	Electrochemical Impedance Spectroscopy
EoL	End of Life
EoW	End of Warranty
HEV	Hybrid Electric Vehicle
LIB	Lithium-ion Battery
LFP	Lithium-iron Phosphate
Min	Minimum
Max	Maximum
PPMCC	Pearson product-moment correlation coefficient
NCA-C	Lithium-nickel-Cobalt-Aluminium-Carbon
P	Parallel configuration
PHEV	Plug-in-Hybrid Electric Vehicle
RC	Resistance-Capacitor
RMS	Root Mean Square value
S	Series configuration
OCV	Open Circuit Voltage

Symbols and units

AhT	Charge-throughput, [Ah]
cov	Covariance, [–]
C	Capacity, [Ah]
(Number) C	C-rate, [A]
Cont	Contribution to ageing, [%]
f	frequency, [Hz]
I	Current, [A]
ΔI	Difference in current between beginning and end of discharge, [A]
R	Resistance, [Ω]
T	Period, [s]
T	Temperature, [$^{\circ}C$]
t	Time, [s]
r	Pearson product-moment correlation coefficient, [–]
SoC	State of charge, [%]
SoI	State of Imbalance, [%]

SoH	State of health, [%]
SoH_E	State of Health based on capacity, [%]
SoH_P	State of Health based on resistance, [%]
ΔSoH_E	Change of State of Health based on capacity, [%]
ΔSoH_P	Change of State of Health based on resistance, [%]
V	Voltage, [V]
V_{oc}	Open circuit voltage, [V]
V_t	Terminal voltage, [V]
#	Number of [–]
σ	Standard deviation [–]

Indices

0	Initial (i.e. time = 0)
eq	Equivalent
f	End
i	Cell number
$init$	Initial
ind	Individual
int	Internal
k	Cycling test
M	Total number of cells connected in parallel, $M = 4$
now	Present value
r	Ratio
$samp$	Sampling
th	Thermal

References

- [1] T. Bruen, J. Marco, Modelling and experimental evaluation of parallel connected lithium ion cells for an electric vehicle battery system, *J. Power Sources* 310 (2016) 91–101, <http://dx.doi.org/10.1016/j.jpowsour.2016.01.001>.
- [2] J. Matras, Quick Test Mini E Battery Electric Car: Run Silent, Run E?, 2010. URL: <http://www.examiner.com/article/quick-test-mini-e-battery-electric-car-run-silent-run-e>.
- [3] Tesla Motors Wiki, Battery Pack, 2014. URL: http://www.teslamotors.wiki/wiki/Battery_Pack.
- [4] A. Farmann, W. Waag, A. Marongiu, D.U. Sauer, Critical review of on-board capacity estimation techniques for lithium-ion batteries in electric and hybrid electric vehicles, *J. Power Sources* 281 (2015) 114–130, <http://dx.doi.org/10.1016/j.jpowsour.2015.01.129>.
- [5] R. Gogoana, M.B. Pinson, M.Z. Bazant, S.E. Sarma, Internal resistance matching for parallel-connected lithium-ion cells and impacts on battery pack cycle life, *J. Power Sources* 252 (2014) 8–13, <http://dx.doi.org/10.1016/j.jpowsour.2013.11.101>.
- [6] X. Gong, R. Xiong, C. Mi, Study of the Characteristics of Battery Packs in Electric Vehicles with Parallel-Connected Lithium-Ion Battery Cells, 2014, <http://dx.doi.org/10.1109/TIA.2014.2345951>.
- [7] N. Yang, X. Zhang, B. Shang, G. Li, Unbalanced discharging and aging due to temperature differences among the cells in a lithium-ion battery pack with parallel combination, *J. Power Sources* 306 (2016) 733–741, <http://dx.doi.org/10.1016/j.jpowsour.2015.12.079>.
- [8] W. Shi, X. Hu, C. Jin, J. Jiang, Y. Zhang, T. Yip, Effects of imbalanced currents on large-format LiFePO₄/graphite batteries systems connected in parallel, *J. Power Sources* 313 (2016) 198–204, <http://dx.doi.org/10.1016/j.jpowsour.2016.02.087>.
- [9] D. Strickland, N. Mukherjee, Second life battery energy storage systems: converter topology and redundancy selection, in: 7th IET International Conference on Power Electronics, Machines and Drives (PEMD 2014), 2014, <http://dx.doi.org/10.1049/cp.2014.0256>, 1.2.02–1.2.02.
- [10] X. Zhao, R.a. De Callafon, L. Shrinkle, Current scheduling for parallel buck regulated battery modules, vol. 19, IFAC, 2014, <http://dx.doi.org/10.3182/20140824-6-ZA-1003.01829>.
- [11] M. Ecker, N. Nieto, S. Käbitz, J. Schmalstieg, H. Blanke, A. Warnecke, D.U. Sauer, Calendar and cycle life study of Li(NiMnCo)O₂-based 18650 lithium-ion batteries, *J. Power Sources* 248 (0) (2014) 839–851, <http://dx.doi.org/10.1016/j.jpowsour.2013.09.143>.
- [12] P. Weicker, A systems approach to Lithium-Ion Mattery Management, Artech House, 2014.
- [13] D. Andre, C. Appel, T. Soczka-Guth, D.U. Sauer, Advanced mathematical methods of SOC and SOH estimation for lithium-ion batteries, *J. Power Sources* 224 (0) (2013) 20–27, <http://dx.doi.org/10.1016/j.jpowsour.2012.10.001>.
- [14] Office for Low Emission Vehicles, Driving the Future Today a Strategy for Ultra Low Emission Vehicles in the UK, 2013. URL: https://www.gov.uk/government/uploads/system/uploads/attachment_data/file/239317/ultra-low-emission-vehicle-strategy.pdf.
- [15] G. Hunt, Electric Vehicle Battery Test Procedures – Rev. 2, United States Advanced Battery Consortium (January).
- [16] J. Arai, Y. Muranaka, E. Koseki, High-power and high-energy lithium secondary batteries for electric vehicles, *Hitachi Rev.* 53 (4) (2004) 182–185.
- [17] B. Kenney, K. Darcovich, D.D. MacNeil, I.J. Davidson, Modelling the impact of variations in electrode manufacturing on lithium-ion battery modules, *J. Power Sources* 213 (2012) 391–401, <http://dx.doi.org/10.1016/j.jpowsour.2012.03.065>.
- [18] A. Barai, G.H. Chouchelamane, Y. Guo, A. McGordon, P. Jennings, A study on the impact of lithium-ion cell relaxation on electrochemical impedance spectroscopy, *J. Power Sources* 280 (2015) 74–80, <http://dx.doi.org/10.1016/j.jpowsour.2015.01.097>.
- [19] W. Waag, S. Käbitz, D.U. Sauer, Experimental investigation of the lithium-ion battery impedance characteristic at various conditions and aging states and its influence on the application, *Appl. Energy* 102 (2013) 885–897, <http://dx.doi.org/10.1016/j.apenergy.2012.09.030>.
- [20] K. Takeno, Quick testing of batteries in lithium-ion battery packs with impedance-measuring technology, *J. Power Sources* 128 (1) (2004) 67–75, <http://dx.doi.org/10.1016/j.jpowsour.2003.09.045>.
- [21] S.F. Schuster, M.J. Brand, C. Campestrini, M. Gleissenberger, A. Jossen, Correlation between capacity and impedance of lithium-ion cells during calendar and cycle life, *J. Power Sources* 305 (2016) 191–199, <http://dx.doi.org/10.1016/j.jpowsour.2015.11.096>.
- [22] The Mathworks Inc., corrcoef, 2015. URL: <http://uk.mathworks.com/help/matlab/ref/corrcoef.html>.
- [23] S. Gupta, Measurement Uncertainties. Physical Parameters and Calibration of Instruments, 2012.